Classification of Human Retinal Microaneurysms Using Adaptive Optics Scanning Light Ophthalmoscope Fluorescein Angiography

Michael Dubow,[1,2] Alexander Pinhas,[1,2] Nishit Shah,[1] Robert F. Cooper,[3] Alexander Gan,[1] Ronald C. Gentile,[1,2,4] Vernon Hendrix,[1] Yusufu N. Sulai,[5] Joseph Carroll,[3,6–8] Toco Y. P. Chui,[1] Joseph B. Walsh,[1] Rishard Weitz,[1] Alfredo Dubra,[3,6,7] and Richard B. Rosen[1,2]

[1]Department of Ophthalmology, New York Eye and Ear Infirmary, New York, New York
[2]Icahn School of Medicine at Mount Sinai, New York, New York
[3]Department of Biomedical Engineering, Marquette University, Milwaukee, Wisconsin
[4]Department of Ophthalmology, Winthrop-University Hospital, Mineola, New York
[5]The Institute of Optics, University of Rochester, Rochester, New York
[6]Department of Ophthalmology, Medical College of Wisconsin, Milwaukee, Wisconsin
[7]Department of Biophysics, Medical College of Wisconsin, Milwaukee, Wisconsin
[8]Department of Cell Biology, Neurobiology and Anatomy, Medical College of Wisconsin, Milwaukee, Wisconsin

Correspondence: Alfredo Dubra, The Eye Institute, 925 North 87th Street, Milwaukee, WI 53226-4812; adubra@mcw.edu.
Richard B. Rosen, New York Eye and Ear Infirmary, 310 East 14th Street, New York City, NY 10003; rrosen@nyee.edu.

Submitted: August 23, 2013
Accepted: December 28, 2013

Citation: Dubow M, Pinhas A, Shah N, et al. Classification of human retinal microaneurysms using adaptive optics scanning light ophthalmoscope fluorescein angiography. *Invest Ophthalmol Vis Sci*. 2014;55:1299–1309. DOI:10.1167/iovs.13-13122

Purpose. Microaneurysms (MAs) are considered a hallmark of retinal vascular disease, yet what little is known about them is mostly based upon histology, not clinical observation. Here, we use the recently developed adaptive optics scanning light ophthalmoscope (AOSLO) fluorescein angiography (FA) to image human MAs in vivo and to expand on previously described MA morphologic classification schemes.

Methods. Patients with vascular retinopathies (diabetic, hypertensive, and branch and central retinal vein occlusion) were imaged with reflectance AOSLO and AOSLO FA. Ninety-three MAs, from 14 eyes, were imaged and classified according to appearance into six morphologic groups: focal bulge, saccular, fusiform, mixed, pedunculated, and irregular. The MA perimeter, area, and feret maximum and minimum were correlated to morphology and retinal pathology. Select MAs were imaged longitudinally in two eyes.

Results. Adaptive optics scanning light ophthalmoscope fluorescein angiography imaging revealed microscopic features of MAs not appreciated on conventional images. Saccular MAs were most prevalent (47%). No association was found between the type of retinal pathology and MA morphology ($P = 0.44$). Pedunculated and irregular MAs were among the largest MAs with average areas of 4188 and 4116 μm^2, respectively. Focal hypofluorescent regions were noted in 30% of MAs and were more likely to be associated with larger MAs (3086 vs. 1448 μm^2, $P = 0.0001$).

Conclusions. Retinal MAs can be classified in vivo into six different morphologic types, according to the geometry of their two-dimensional (2D) en face view. Adaptive optics scanning light ophthalmoscope fluorescein angiography imaging of MAs offers the possibility of studying microvascular change on a histologic scale, which may help our understanding of disease progression and treatment response.

Keywords: microaneurysm, AOSLO, fluorescein angiography

Initially described in diabetes, MAs appear as manifestations of a wide range of systemic and retinal diseases, including ischemic, infectious, inflammatory, hematologic, and radiation-related disorders.[1–5] Retinal MAs have been shown to be an important sign in the progression of systemic disease,[6–12] and they have been used as components of multiple retinopathy severity classification schemes.[13–16] Microaneurysm counting[17–21] and dynamic turnover[22–25] studies have revealed associations linking MAs to increased retinopathy, suggesting that even a single MA may have predictive value.[26] Furthermore, clinical imaging has demonstrated that MAs are correlated with extravascular leakage and vision loss.[23,27]

Despite their clinical significance, the pathogenesis and natural history of individual MAs remains poorly understood. Histologic studies using India ink infusion and trypsin digest techniques have investigated the role of pericytes,[28,29] lipid and hyaline infiltration,[2,30] neovascularization,[31] and endothelial disruption[32] in attempts to understand MA formation and progression. The relationship between the MA wall and lumen has been investigated using trypsin digest processing,[33] electron microscopy,[34] and confocal scanning laser microscopy with von Willebrand factor staining.[35] One recent study has suggested that MA radius-to-associated-vessel-diameter ratio may be a useful metric for stratifying risk of leakage,[36] helping to explain why some smaller MAs lead to leakage while some

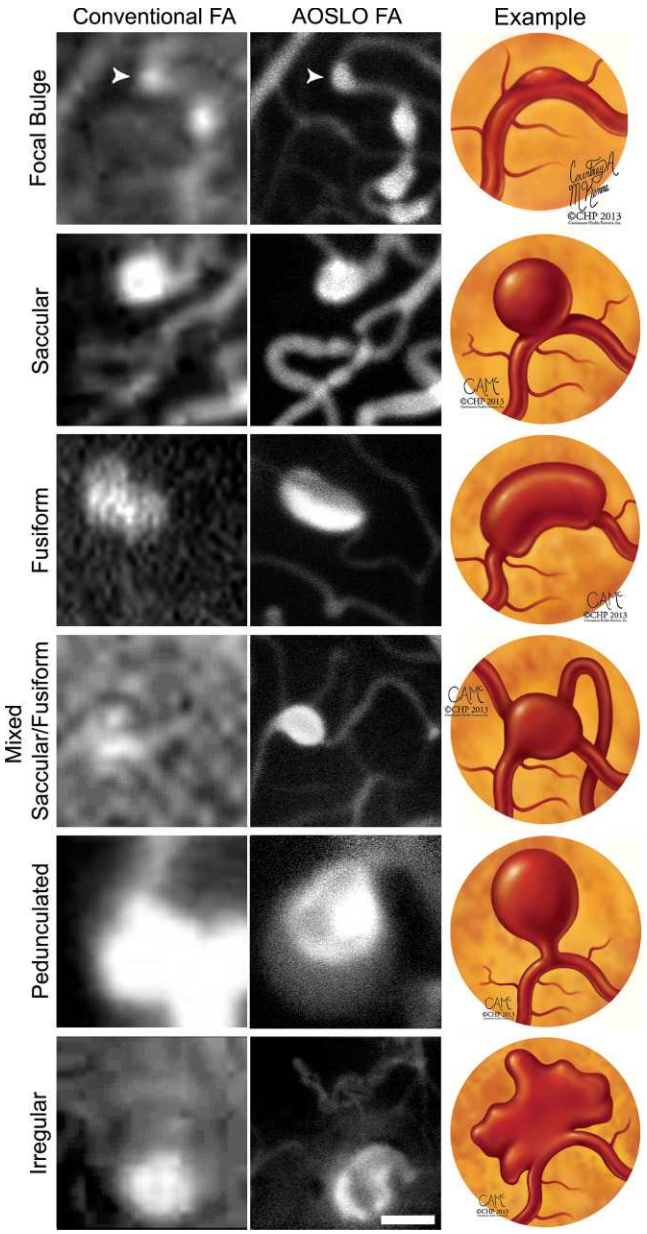

FIGURE 1. Proposed expanded anatomical classification of MAs as seen with conventional fluorescein angiography (*left*) and AOSLO FA (*center*) with corresponding illustrated examples (*right*). All images have been contrast stretched. *Scale bar*: 50 μm.

larger ones do not. As treatment modalities advance to target individual MAs with laser therapy,[37] the ability to determine which MAs are at higher risk for leakage or rupture is increasingly valuable. However, since most MA knowledge is derived from post mortem histopathology, we currently have a very limited understanding of the dynamics of MA development and natural progression in vivo.

Advances in retinal imaging have increased our ability to image the retinal vasculature, including the development of time-differential fundus photography,[38–40] optical coherence tomography (OCT),[41–46] and entoptic viewing.[47–49] A recent study using spectral-domain OCT (SD-OCT) was able to extract basic MA dimensions through diameter measurements.[50] The correction of the ocular monochromatic aberrations using adaptive optics, when added to the fundus camera,[51,52]

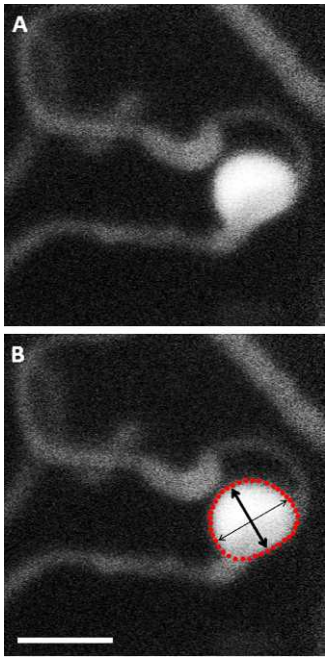

FIGURE 2. Adaptive optics scanning light ophthalmoscope fluorescein angiography image of saccular MA (**A**) with schematic (**B**) depicting manual boundary segmentation of aneurysm in order to determine area (within *red dotted lines*), perimeter (*red dotted line*), feret max (*thin arrow*), and feret min (*thick arrow*). *Scale bar*: 50 μm.

scanning light ophthalmoscope (AOSLO),[53–57] and OCT (AO-OCT),[58,59] has further improved our capacity to study healthy and diseased microvasculature anatomy. Recently, we demonstrated that in vivo imaging of the healthy human retinal microvasculature could be performed with safe light levels by combining AOSLO with fluorescein angiography (AOSLO FA).[60]

Studying MAs with the resolution of AOSLO technology has the potential to reveal helpful information about their formation, natural progression, and response to treatment. In this manuscript, we use AOSLO FA to expand upon previous MA classification schemes[35,52] and to introduce qualitative and quantitative metrics to describe MA geometry in vivo. Using the complementary aspect of AOSLO reflectance imaging, we investigated MA capillary wall and lumen relationships as well as regions of MA and capillary nonperfusion. The associations between MA morphology, size, and luminal fluorescence were evaluated statistically.

METHODS

Human Subjects

To ensure that the MA classification scheme presented here was comprehensive and applicable to different pathologies, subjects with various vascular retinopathies and ophthalmic treatment histories were recruited. Ophthalmic diagnoses were established for each patient based upon review of their medical records by New York Eye and Ear Infirmary ophthalmologists. The presence of retinal MAs had been previously documented by color fundus photography (Topcon 3D OCT 2000; Topcon Corporation, Tokyo, Japan) and/or standard FA (Topcon 3D OCT 2000; Topcon Corporation; Optos P200; Optos plc, Dunfermline, Scotland; and Heidelberg Spectralis HRA-OCT; Heidelberg Engineering, Inc., Heidelberg, Germany). Following discussion of the nature and possible consequences of the

Table 1. Patient Demographics

Patient ID	Diagnosis	Age, y	Sex	Eye	Race/Ethnicity	Ophthalmic Treatment History
RR_0067	CRVO	51	M	OS	White	Anti-VEGF ×1
RR_0072	DR	52	M	OD	Hispanic	PRP
RR_0084	DR	48	M	OD	African-American	No treatment
RR_0086	DR	46	F	OD	Hispanic	PRP, anti-VEGF ×3
RR_0095	HTN	47	M	OD	Hispanic	No treatment
RR_0099	BRVO	55	F	OS	White	No treatment
RR_0120	DR	68	M	OS	Hispanic	PRP
RR_0129	BRVO	54	F	OS	African-American	No treatment
RR_0148	DR	53	F	OS	Hispanic	Focal laser
RR_0149	CRVO	44	M	OD	White	Anti-VEGF ×2
RR_0151	CRVO	64	F	OS	Hispanic	Anti-VEGF ×8
RR_0167	DR	49	F	OU	White	No treatment
RR_0182	CRVO	55	M	OD	White	Anti-VEGF ×6

PRP, pan-retinal photocoagulation.

study, informed written consent was obtained from each subject. This study adhered to the tenets of the Declaration of Helsinki and was approved by the institutional review board of the New York Eye and Ear Infirmary.

AOSLO Imaging Protocol

Mydriasis and cycloplegia were achieved by instillation of one drop of 2.5% phenylephrine hydrochloride ophthalmic solution (Bausch & Lomb, Inc., Rochester, NY) and one drop of 1% tropicamide ophthalmic solution (Akorn, Inc., Lake Forest, IL). Ocular axial length measurements were collected (IOL Master; Carl Zeiss Meditec AG, Jena, Germany) in order to calculate the scale of the AOSLO images using the Emsley schematic eye model.[61] The AOSLO used in this study was a modified version of the one originally described by Dubra and Sulai[62] with the addition of a 488-nm light source, an emission filter centered at 525 nm, and a 45-nm transmission bandwidth. The subjects were positioned in front of the instrument using a dental impression made with dental putty (Splash! Putty; DenMat Holdings, LLC, Lompoc, CA) on a bite bar mounted on a translation stage. Fine adjustments of the stage allowed for stable and repeatable alignment of the subject's pupil with the entrance pupil of the AOSLO (7.75 mm in diameter). Subjects were instructed to direct their gaze toward an internal fixation target that was moved until the desired region of interest was within the AOSLO field of view. These areas, all located within 15° from the center of the fovea, contained microangiopathic features previously identified on color fundus photography and/or standard FA. The reflectance channel was used to scout important regions to be examined with the fluorescence channel following fluorescein administration.

Adaptive optics scanning light ophthalmoscope fluorescein angiography imaging was performed using our previously described protocol,[60] after administering fluorescein at 20 mg/kg of body weight in 50 mL of orange juice. Imaging was initiated at 15 minutes following ingestion. Simultaneous image sequences of fluorescence and reflectance images, consisting of up to 500 frames each, were recorded at 15 frames/s using either a 1.0°, 1.5°, or 1.75° field of view. Subjects were given short breaks at regular intervals and encouraged to blink frequently to maintain normal tear film. Imaging sessions concluded once all regions of interest had been imaged, the patient tired, or the image signal waned. No imaging session extended longer than 45 minutes. The feasibility of studying MA dynamics was explored through longitudinal imaging at 1-month intervals in two subjects.

Light Safety

During AOSLO imaging, the retina was simultaneously scanned with three light sources, with wavelengths centered at 488, 790, and 850 nm. These light sources were coaxial and entered the eye with collimation accounting for the longitudinal chromatic aberration of an average eye. The three beams overlapped producing a square raster, 30% larger than the imaged area, using a 14.5-KHz horizontal resonant optical scanner (Electro-Optical Products Corporation, New York, NY) and a 16-Hz vertical scanner (Physik Instrumente, Karlsruhe, Germany). Synchronous modulation of the light sources turned them on at the beginning of each horizontal line used for imaging when scanning from left to right. As a result, only the central portion of the scanning raster was exposed to light. The optical powers without modulation (i.e., continuous wave) measured at the cornea were 15 μW for the 850-nm wavefront sensing superluminescent diode (SLD; Superlum, Carrigtwohill, Ireland), 210 μW for the 790-nm imaging SLD (Superlum), and 32 μW for the 488-nm diode laser (Lasos, Lasertechnick GmbH, Jena, Germany). During imaging, the on/off modulation reduced the average powers delivered by approximately 75%. No retinal location was exposed to the combined light sources for longer than 120 seconds. All sources were considered as lasers for calculating maximum permissible exposure (MPE) under the American National Standards I (ANSI) Z136.1 2000 guidelines.[63] These imaging parameters, as described above, resulted in light exposures six times below both the photochemical and the thermal MPE limits. In order to avoid any possibility for light or fluorescein toxicity, repeat imaging sessions were performed after at least a 7-day interval.

Image Processing

The reflectance image sequences, collected using 790-nm light, were used to estimate eye motion[64] in order to create a single

Table 2. Distribution of MA Morphology in Each Pathology Imaged

	FB	S	F	M	P	I
CRVO	8	15	6	1	1	1
HTN	2	4	2	2	0	1
BRVO	2	6	3	0	1	1
DR	2	19	2	7	2	5
Total, %	15	47	14	11	4	9

FB, focal bulge; S, saccular; F, fusiform; M, mixed; P, pedunculated; I, irregular.

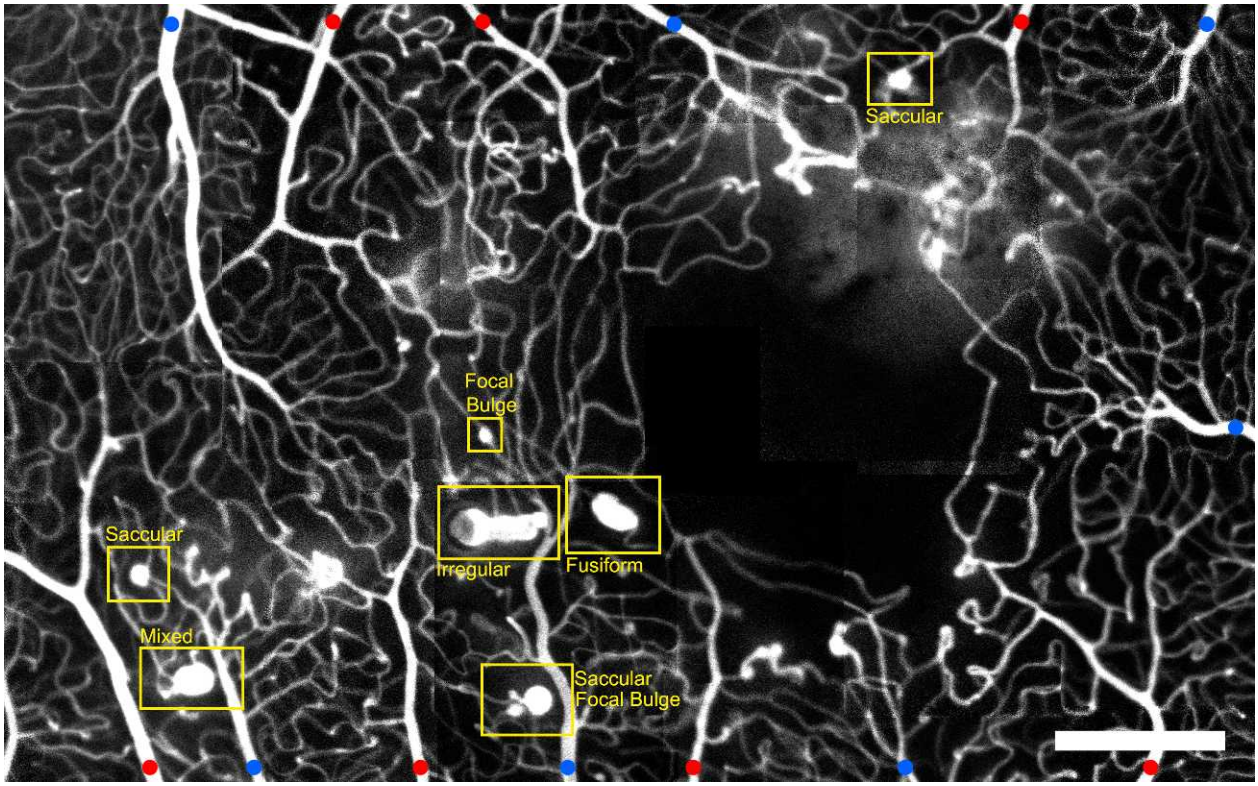

FIGURE 3. Montage of AOSLO FA images, showing the foveal capillary network and the foveal avascular zone (FAZ) in the right eye of a subject with hypertension. Microaneurysms of various size and morphology are visible. *Red dots* indicate arterioles. *Blue dots* indicate venules. *Scale bar*: 300 μm.

registered average image with high signal-to-noise ratio from each image sequence. The AOSLO reflectance and fluorescence images included in this manuscript were created in this manner, using sequences of 32 to 100 frames after compensation of the warping due to the sinusoidal motion of the resonant scanner. Registered images were manually tiled (Adobe Photoshop CS6; Adobe Systems, Inc., San Jose, CA) to create larger montages of the retinal vasculature, as needed.

Microaneurysm Classification

The qualitative morphologic classification of MAs proposed in this work is an extension of the scheme suggested by Moore et al.[35] Reflectance AOSLO images were often obscure in subjects with extensive vascular pathology, preventing interpretable visualization of vascular features, while AOSLO FA was often able to clarify these complex vascular relationships. The variation in longitudinal chromatic aberration across individuals prevented both reflectance and fluorescence images from being in focus at the same time for all subjects.

There were 93 MAs identified and classified according to their two-dimensional (2D) geometry in the en face AOSLO FA images (Fig. 1), as follows:

1. Focal bulge were defined as MAs where the combined width of the associated capillary and MA was less than twice the width of an adjacent nonaffected region of the capillary. All other morphologies represented MAs where the combined width of the associated capillary and MA was more than twice the width of an adjacent nonaneurysmal region.
2. Saccular MAs were defined as those with asymmetric dilatations with at least 75% of the total area of the MA on one side of the central axis of the associated capillary.

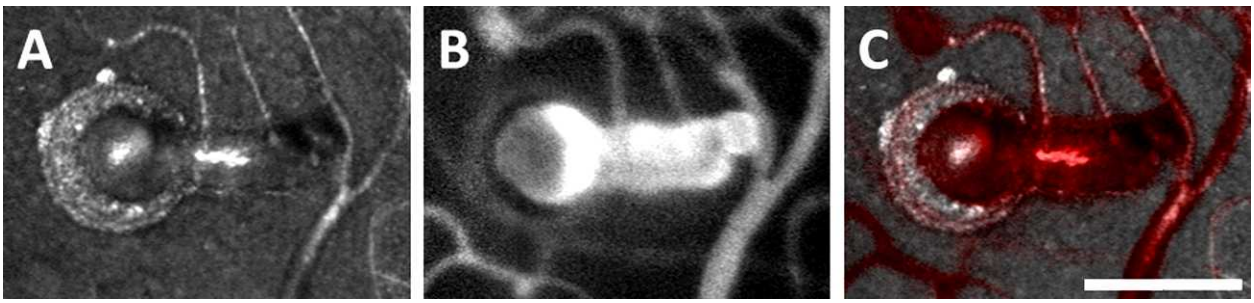

FIGURE 4. Adaptive optics scanning light ophthalmoscope reflectance (**A**) and fluorescence (**B**) images of an irregular MA, nasal to FAZ in Figure 3. The superposition of these images ([**C**], with [**B**] in *red*) shows the relationship between wall and lumen. *Scale bar*: 100 μm.

Investigative Ophthalmology & Visual Science

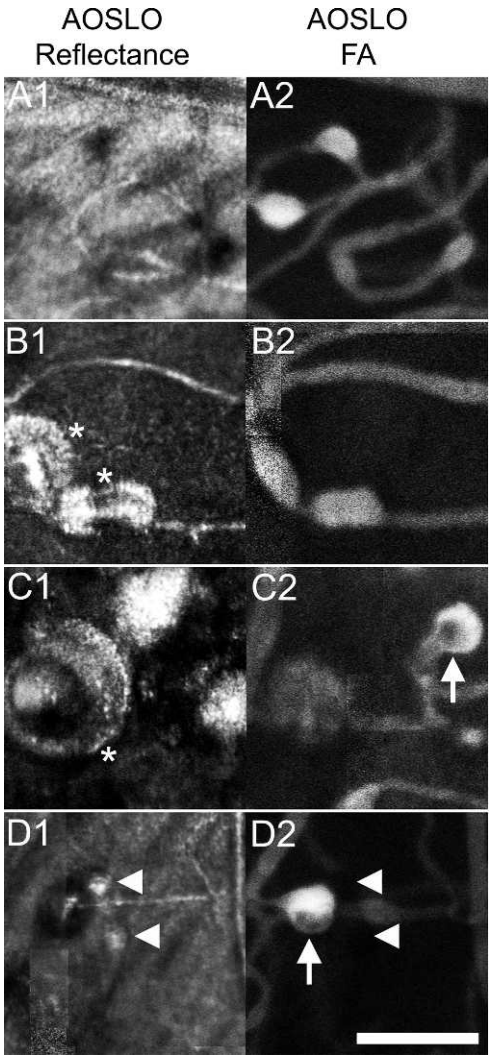

Figure 5. Reflectance AOSLO images (*left*) and AOSLO FA (*right*) of pathologic regions in a patient with CRVO reveal various states of MAs. Hyperfluorescent saccular and fusiform MAs (**A2**) were visualized in a region without additional pathology (**A1**). *Asterisks* (**B1**, **C1**) indicate thickened vascular walls that were seen in both hyperfluorescent MAs (**B2**) and a hypofluorescent MA (**C2**). *Arrows* (**C2**, **D2**) indicate intraluminal hypofluorescence. *Carets* (**D1**, **D2**) depict location of small MAs that do not fluoresce on AOSLO FA. *Scale bar*: 100 μm.

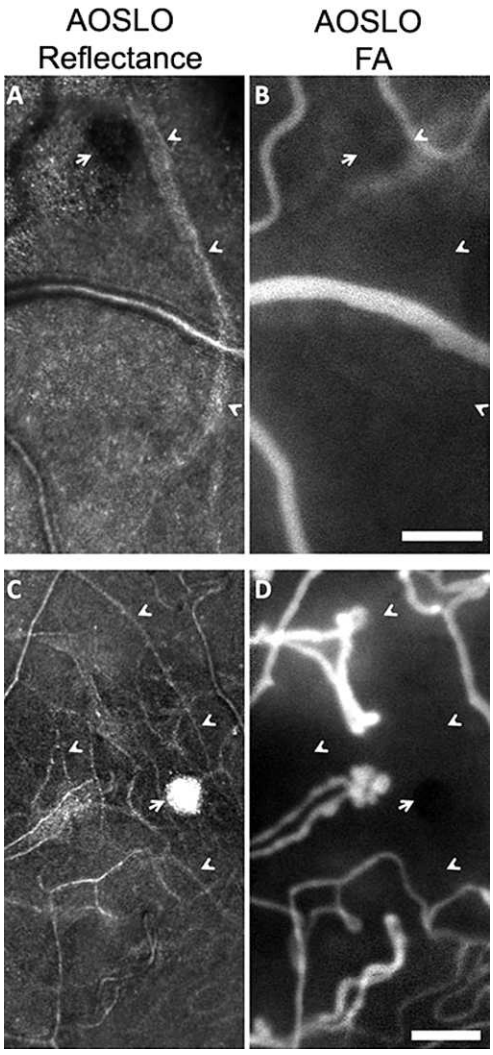

Figure 6. Reflectance AOSLO images (*left*) and AOSLO FA (*right*) of pathologic regions in two patients. In both patients, reflectance AOSLO images reveal the physical remnant of a MA (adjacent to *arrows*) attached to an arteriole (**A**) or a capillary (**C**). *Carets* show capillaries visible on reflectance channel (**A**, **C**) that are hypofluorescent and not perfused on AOSLO FA (**B**, **D**). (**A**, **B**) are from a subject with BRVO and (**C**, **D**) are from a subject with proliferative DR. *Scale bar*: 100 μm.

3. Fusiform MAs were defined as symmetrically dilated MAs around their associated capillary, with less than 75% of the total area of the MA on either side of the associated capillary.
4. Mixed saccular/fusiform were defined as MAs that could not be categorized as either saccular or fusiform and it was uncertain which capillary was associated with it, or when the orientation of the MA prevented a clear en face view.
5. Pedunculated MAs were asymmetric MAs tethered to their associated capillary via a tapered narrowing of the lumen.
6. Irregular MAs were saccular, fusiform, or pedunculated with a nonconvex shape (note: a convex shape is one in which the line segment defined by any two points within it is fully contained within the shape). For pedunculated MAs, this definition excludes the region associated with the tapered narrowing of the lumen and applies to the remainder of the aneurysm.

As MA features appear different in AOSLO FA and reflectance images, comparing the two techniques allows inferences to be made about capillary walls and perfusion. Reflectance AOSLO images typically reveal the capillary and MA wall, while AOSLO FA shows exclusively the intraluminal, perfused space. Accordingly, AOSLO reflectance images were used to locate nonperfused capillaries, which did not appear in AOSLO FA. With AOSLO FA, the presence of focal hypofluorescent regions within the otherwise highly fluorescent lumen of the MA was recorded.

Three trained examiners familiar with the MA classification (Fig. 1) independently graded all 93 MAs. Based on their classifications, interexaminer agreement was quantified by calculating the Fleiss' kappa reliability coefficient.[65]

Investigative Ophthalmology & Visual Science

Table 3. Pathology Versus MA Quantitative Metrics

	Area, $\mu m^2 \pm$ SD	Perimeter, $\mu m \pm$ SD	Feret max, $\mu m \pm$ SD	Feret Min, $\mu m \pm$ SD
CRVO	1400 ± 1000	190 ± 120	65 ± 39	51 ± 33
HTN	2000 ± 1500	280 ± 170	97 ± 61	66 ± 36
BRVO	2500 ± 2100	280 ± 210	92 ± 64	77 ± 62
DR	2200 ± 1500	300 ± 160	100 ± 57	77 ± 40
Mean	1900 ± 1500	250 ± 160	87 ± 55	67 ± 42
Range	400–7400	77–380	29–130	19–97

Microaneurysm Geometry Quantification

The boundaries of all 93 MAs were manually segmented on the 2D AOSLO FA images using custom MATLAB (Mathworks, Natick, MA) software. The area, perimeter, feret maximum (longest intraluminal diameter of MA), and feret minimum (longest diameter perpendicular to feret maximum) of these boundaries were then calculated (Fig. 2). Traditionally, MA measurements have frequently used width of the aneurysm along the direction perpendicular to the associated capillary. That requires identifying, with certainty, the capillary associated with each MA and determining the location and extent of that capillary's connection with the MA, which is not always possible. Feret maximum (max) and minimum (min) were therefore selected instead, as they can be more readily measured even when information surrounding the associated capillary was not clear.

Correlations between metrics, primary ophthalmic diagnoses, and morphologies were studied by performing a two-step analysis. First, ANOVA tests were used to test whether there were significant differences among the metrics derived from each of the conditions and morphologies. When these tests showed significance ($P < 0.05$), then the Scheffe's post hoc test was used to evaluate the differences between each possible pair of variables examined.

Interobserver segmentation reliability was assessed by having three trained, independent examiners segment the boundary of 14 randomly selected MAs. Then, intraclass correlation of their measurements was calculated.

Results

Patient Demographics

Included in this study were 13 subjects (7 men, 6 women; mean age 52.8 years; range, 44–68 years) from various racial/ethnic backgrounds (Table 1). Ophthalmic diagnoses, included diabetic retinopathy (DR) in six patients, central retinal vein occlusion (CRVO) in four patients, branch retinal vein occlusion (BRVO) in two patients, and hypertensive retinopathy (HTN) in one patient. One DR subject had imaging performed in both eyes.

Morphology and Pathology

Among the six morphologies, saccular MAs were the most prevalent, followed by focal bulge, fusiform, mixed, irregular, and pedunculated, respectively (Table 2). No relationship was seen between systemic pathology and MA morphology (ANOVA, $P = 0.44$). This is consistent with the fact that even when imaging a relatively small retinal area affected by a single pathology, as shown in Figure 3, multiple types of MAs were simultaneously present. Interobserver morphology identification agreement among the three readers was high (kappa coefficient: 0.88).

Table 4. Significance Levels (Scheffe's Method) of Quantitative Metrics Between Pathologies

	CRVO	HTN	BRVO
Area			
HTN	0.64		
BRVO	0.12	0.87	
DR	0.17	0.99	0.89
Perimeter			
HTN	0.45		
BRVO	0.40	1.00	
DR	**0.05**	0.99	0.99
Feret max			
HTN	0.40		
BRVO	0.50	1.00	
DR	**0.05**	0.96	0.99
Feret min			
HTN	0.75		
BRVO	0.28	0.94	
DR	*0.07*	0.91	1.00

Y greater than X, statistically significant results bolded, nearly statistically significant results italicized.

Wall and Lumen

Imaging using AOSLO reflectance and FA provide complementary information about capillary wall and lumen (Fig. 4). The combination of these imaging modalities revealed that, even within a single eye affected by a single condition, MAs with varying degrees of wall thickening and fluorescence could be observed (Fig. 5, subject with CRVO). Reflectance AOSLO imaging can also reveal evidence of nonperfused capillaries and obliterated MAs that cannot be visualized with AOSLO FA imaging alone (Fig. 6).

Pathology and MA Geometrical Metrics

Interobserver segmentation reliability among the three readers was high (intraclass correlation: 0.99). There was a significant difference between the mean metric values estimated for MAs from each disease (Table 3) for area ($P = 0.05$, ANOVA), perimeter ($P = 0.04$, ANOVA), feret max ($P = 0.05$, ANOVA), and feret min ($P = 0.05$, ANOVA). Further analysis using the Scheffe test, summarized in Table 4, failed to find statistically significant differences between all possible pairs of systemic pathologies. Statistical significance ($P < 0.05$) and near statistical significance ($0.05 < P < 0.10$) was found only between CRVO and DR for perimeter, feret max, and feret min. Bubble graphs (Fig. 7A) show the similarity of quantitative metrics between pathologies.

Morphology and MA Geometrical Metrics

Among the six MA morphologies, there were significant difference between their mean measurements of area ($P = 0.0001$, ANOVA), perimeter ($P = 0.0001$, ANOVA), feret max ($P = 0.0001$, ANOVA), and feret min ($P = 0.0001$, ANOVA) (Table 5). Further analysis using the Scheffe test (Table 6), found differences between several pairs of morphologies. Several statistical significant ($P < 0.05$) and nearly statistically significant ($0.05 < P < 0.10$) results were found for the greater perimeter, feret max, and feret min of pedunculated

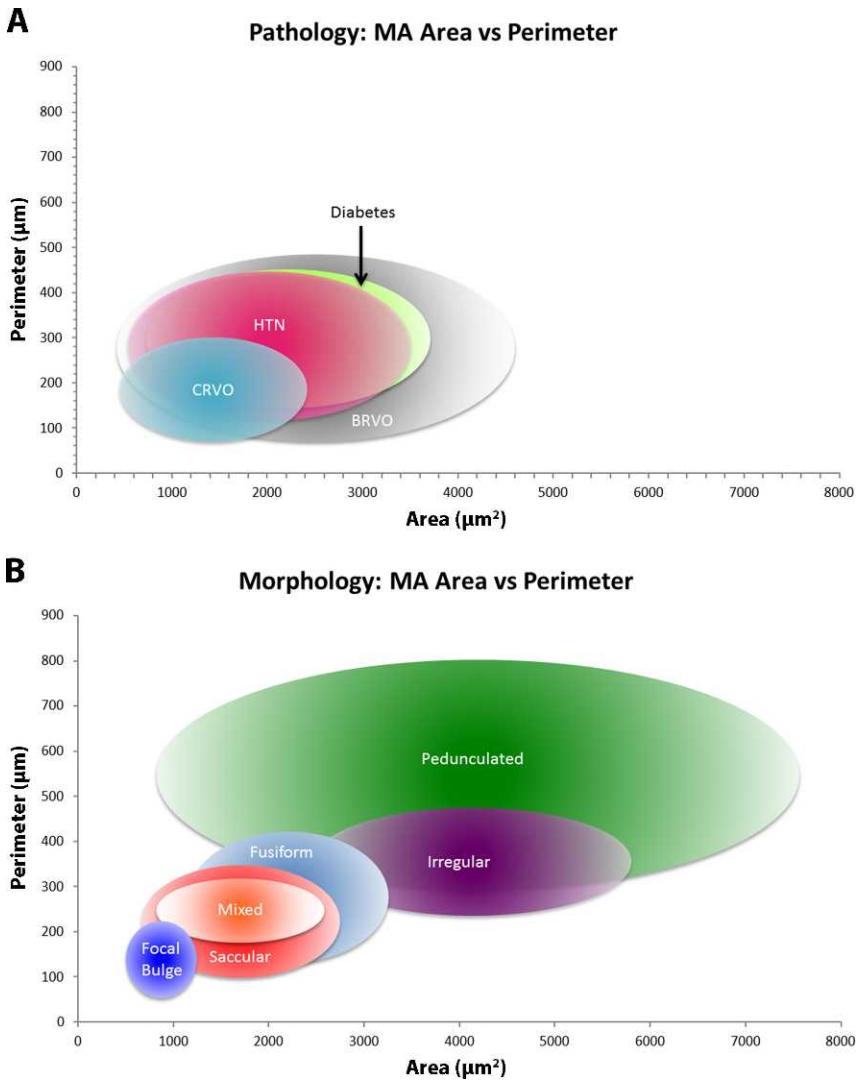

FIGURE 7. Graphs comparing quantitative metrics (area versus perimeter) for pathologies (**A**) and morphologies (**B**). Center point of each ellipse represents area mean (*x*-axis) and perimeter mean (*y*-axis). Horizontal extent of ellipses determined by area mean ± SD. Vertical extent of ellipses determined by means of perimeter ± SD.

and irregular MAs as compared with the other morphologies. Bubble graphs (Fig. 7B) show the differences of quantitative metrics between morphologies.

Intraluminal Hypofluorescent Regions Versus Morphology and Quantitative Metrics

Adaptive optics scanning light ophthalmoscope fluorescein angiography images revealed intraluminal hypofluorescence in 28 out of 93 (30.1%) MAs (Fig. 1, AOSLO FA fusiform, irregular, pedunculated; Fig. 4B; Figs. 5C2, 5D2, boxes). This hypofluorescence was never found in focal bulge MAs (0%), often found in saccular (25%), fusiform (30%), mixed (50%), and pedunculated (50%), and most frequently in irregular MAs (75%). Microaneurysms with hypofluorescent regions were statistically (ANOVA) larger in area (3086 vs. 1448 µm², $P = 0.0001$), perimeter (358 vs. 209 µm, $P = 0.0001$), feret max (121 vs. 73 µm, $P = 0.0001$), and feret min (96 vs. 54 µm, $P = 0.0001$). Although there was no correlation between systemic pathology and intraluminal hypofluorescence (ANOVA, $P = 0.68$), there was a strong correlation between the presence or absence of hypofluorescent regions and the various morphologies (ANOVA, $P = 0.0001$).

Longitudinal Imaging

A fusiform retinal MA (Fig. 8, left column) in a subject with hypertensive retinopathy (Fig. 3) was shown to remain unchanged over a 4-month period (variability of each metric was <±2% throughout). An adjacent retinal region, imaged only at time 0 and again after 4 months (Fig. 8, middle column),

TABLE 5. MA Morphology Versus Quantitative Metrics

	Area, µm² ± SD	Perimeter, µm ± SD	Feret Max, µm ± SD	Feret Min, µm ± SD
FB	840 ± 370	150 ± 100	50 ± 34	40 ± 24
S	1700 ± 1000	220 ± 120	74 ± 41	62 ± 36
F	2200 ± 1100	300 ± 170	110 ± 5	67 ± 36
M	1700 ± 900	260 ± 120	91 ± 40	69 ± 27
P	4200 ± 3400	560 ± 260	190 ± 81	160 ± 80
I	4100 ± 1700	390 ± 140	140 ± 52	92 ± 41

Table 6. Significance Levels (Scheffe's Method) of Quantitative Metrics Between Morphologies

	FB	S	F	M	P
Area					
S	0.39				
F	0.16	0.91			
M	0.48	1.00	0.91		
P	**0.001**	**0.01**	0.13	**0.04**	
I	**0.001**	**0.001**	**0.03**	**0.005**	1.00
Perimeter					
S	0.65				
F	0.14	0.67			
M	0.48	0.97	0.99		
P	**0.001**	**0.001**	**0.05**	**0.02**	
I	**0.008**	*0.07*	0.79	0.58	0.5
Feret max					
S	0.74				
F	*0.07*	0.35			
M	*0.5*	0.95	0.97		
P	**0.001**	**0.002**	0.15	**0.04**	
I	**0.006**	**0.04**	0.88	**0.006**	0.69
Feret min					
S	0.55				
F	0.57	0.99			
M	0.48	0.99	1.00		
P	**0.001**	**0.001**	**0.04**	**0.009**	
I	*0.07*	0.45	0.79	0.87	0.15

Y greater than X, statistically significant results bolded, nearly statistically significant results italicized.

shows an MA with mixed shape that dramatically increased in size adjacent to a focal bulge MA that regressed over the same time. Imaging in a subject with CRVO before and after anti-VEGF injection shows regression of a mixed MA that was sustained 3 months later (Fig. 8, right column), while an adjacent, saccular MA remained stable.

Discussion

Emerging high-resolution ophthalmic imaging modalities such as AOSLO and motion contrast OCT are allowing for the visualization of retinal capillaries with unprecedented transverse and axial resolution. When used to image retinas affected by vascular disease, AOSLO FA reveals MAs with great detail, permitting a rich morphologic categorization scheme. The retinal MA classification presented in this work is based on the en face, 2D geometry of MAs. It incorporates the saccular, fusiform, and focal bulge designations proposed in previous studies,[35,52] as well as three additional morphologies discernable with AOSLO FA. Although our proposed classification is based on AOSLO FA images, it can be applied to MA images acquired using other modalities, such as emerging motion contrast techniques.[53–55,57,66–69]

This study is limited by the relatively small number of MAs from 13 patients representing a variety of retinal conditions and ophthalmic treatment histories. Additionally, our analysis attempted to classify MAs, which are three-dimensional (3D) structures, based solely upon their 2D, en face appearance. This may have limited our accuracy in geometrical assessment and will need to be validated using additional techniques. Three-dimensional imaging modalities with isotropic or near-isotropic resolution (e.g., AO-OCT) might help to reveal additional complexities of MA structure, including the nature

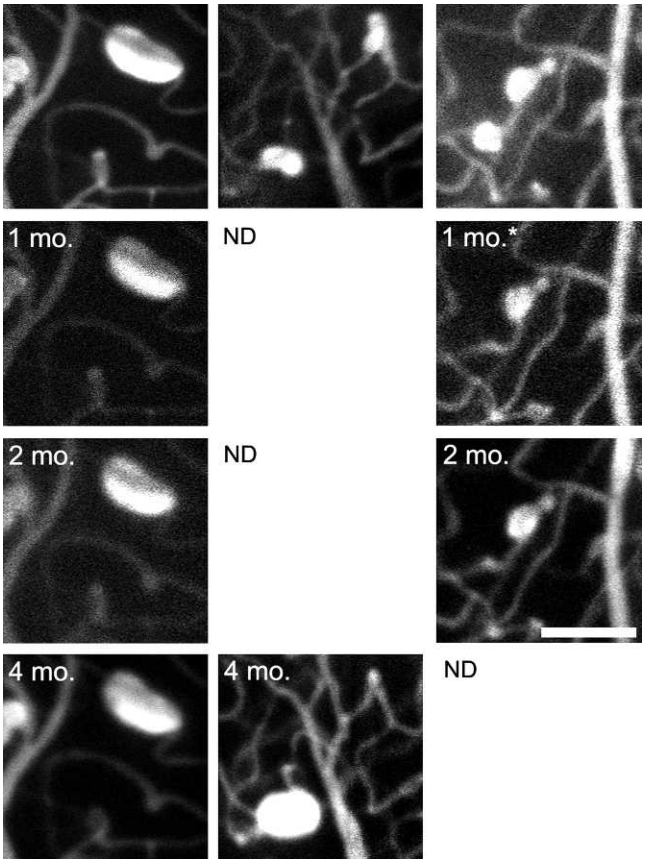

Figure 8. *Left* and *center columns* from one subject with hypertensive retinopathy; *right column* from one subject with CRVO. *Left column* shows AOSLO FA images of a fusiform MA with stable boundaries at four different imaging sessions over a 4-month period. *Center column* follows a mixed MA with growth between time 0 (perimeter: 162 μm, area: 1702 μm^2, feret max: 52 μm, feret min: 57 μm) and a second imaging session at 4 months (perimeter: 230 μm, area: 3676 μm^2, feret max: 63 μm, feret min: 77 μm). The initial image shows a focal bulge MA in the *upper right corner* that appears to have regressed by the later session. *Right column* depicts a region with saccular (perimeter: 145 μm, area 1415 μm^2, feret max: 52 μm, feret min: 39 μm) and mixed MAs (perimeter: 120 μm, area 1030 μm^2, feret max: 40 μm, feret min: 35 μm) imaged before and after anti-VEGF treatment (*asterisk* indicates treatment had occurred 3 weeks prior). The mixed MA regressed and continued to be hypofluorescent at an additional follow-up imaging session while the saccular MA remained stable. *Scale bar*: 100 μm. ND, no data.

of mixed morphology MAs. With all of these limitations considered, the data resulting from the classification and boundary-derived metrics provides a number of interesting, early findings.

The first observations derived from statistical testing was that retinal pathology appeared to place no limits or bias to development of MA morphology, and that multiple, if not all, MA morphologies can be found within an adjacent, small area of an individual retina. Thus, while assaying for the presence of MAs may be a sensitive tool for following retinal pathology, MA morphology does not seem to have a propensity for any vasculopathy. Consistent with a previous study in DR,[35] we found that saccular MAs were more prevalent than fusiform and focal bulge morphologies; this trend applied not only to DR, but also to the subjects with CRVO, BRVO, and HTN.

An initial ANOVA test indicated that the mean metric values are different among the retinal conditions tested in this work (P = 0.04–0.05). However, Scheffe tests used to evaluate

differences in metric values between any pair of pathologies only showed that diabetic MAs had statistically greater ($P < 0.05$) mean perimeter and feret max than CRVO MAs. Thus, based on the metrics used in this study, there are few obvious differences between MAs due to retinal pathology. In contrast, the different types of MA morphologies show several, more statistically significant differences in some cases, including the relatively greater size of irregular and pedunculated morphologies and the smaller dimensions of the focal bulge MAs. This is expected as the classification itself is, like these metrics, based on the MA geometry. Future studies will be needed to further elaborate on the differences between the pathologies and morphologies presented here.

A recent study by Wang et al.[50] found no correlation between MA leakage and lumen diameter, wall diameter, or wall thickness, suggesting that increasing size may not lead to increased risk of leakage. Ezra et al.[36] found that the physical relationship between the MA radius and associated vessel wall may contribute to leakiness in saccular MAs. Several neuroradiology studies have found that multilobular intracranial aneurysms are more likely to rupture than unilobular aneurysms,[70–72] with one group determining that aneurysm neck diameter and not overall aneurysm size was more important in determining the risk of rupture.[73] These studies indicate that size alone is not a sufficient predictor for course of MA pathology, and that other metrics may need to be identified. It is likely that a deeper understanding of MA morphology may help determine the risk of leakiness or rupture.

In addition to determining boundaries, AOSLO FA reveals intraluminal hypofluorescent regions within some larger MAs. These regions, not readily observable using conventional FA, appeared in almost one-third of the imaged MAs, irrespective of the underlying retinal condition. Notably, such hypofluorescent areas were absent in focal bulge MAs, but appeared in the majority of the pedunculated and irregularly shaped ones. Histologic studies have revealed that MA lumens can be infiltrated by a variety of cell types, ranging from acute inflammatory cells such as polymorphonuclear cells and monocytes to red blood cell breakdown products and cellular debris.[34] The hypofluorescence we observed could represent such luminal clots. The greater luminal surface area of larger MAs like the pedunculated and irregular morphologies may produce more turbulent blood flow, which may increase the risk of endothelial injury and the formation or enlargement of luminal clots. Further studies are needed to elucidate the relationship between these hypofluorescent regions and advanced disease.

The complementary information provided by reflectance AOSLO and FA imaging proved useful in evaluating wall thickness and identifying nonperfused capillaries and MAs. The different perspective provided by each imaging modality was helpful in exploring MA natural progression. This was further examined via imaging a few MAs longitudinally (Fig. 8), demonstrating that AOSLO FA can show MA stability, growth, and resolution as well as potentially evaluate the efficacy of various treatments. The observation of MAs in various stages of resolution only a few microns apart on the same capillary illustrates a complex dynamic at play. While the regression of an MA following anti-VEGF treatment (Fig. 8, right column) is encouraging, it remains to be seen whether the regression was due to treatment or just coincident to natural history. As such, monitoring a small sample of MAs, or their turnover, may not accurately portray all possible patterns of progression or treatment response. With additional work beyond this preliminary study, the AOSLO FA may prove to be a powerful tool in studying the treatment effects of anti-VEGF interventions on MAs.

Combining a robust qualitative classification with quantitative metrics may allow us to better stratify MAs clinically in terms of risk of leakage or rupture and associated capillary dropout. Clinical applications of this approach may prove useful in better understanding microvascular disease progression and help point the way to more successful treatment regimes.

Acknowledgments

The authors thank Courtney McKenna for her illustration assistance and Eric Cheang, Chun Lin Liu, Jae Ahn, Mathew Birnbaum, Lenny Rostomian, Ahmad Rehmani, and Moataz Razeen for their assistance with image processing.

Supported by the Shelley and Steven Einhorn Clinical Research Center; grants from the Marrus Family Foundation, Bendheim-Lowenstein Family Foundation, Wise Family Foundation, Edith C. Blum Foundation, and Chairman's Research Fund of the New York Eye and Ear Infirmary; National Institutes of Health Grants P30EY001931 and UL1TR000055; an unrestricted departmental grant from Research to Prevent Blindness; the Glaucoma Research Foundation; a Career Development Award from Research to Prevent Blindness; and a Career Award at the Scientific Interface from the Burroughs Wellcome Fund (AD).

Disclosure: **M. Dubow**, None; **A. Pinhas**, None; **N. Shah**, None; **R.F. Cooper**, None; **A. Gan**, None; **R.C. Gentile**, None; **V. Hendrix**, None; **Y.N. Sulai**, None; **J. Carroll**, None; **T.Y.P. Chui**, None; **J.B. Walsh**, None; **R. Weitz**, None; **A. Dubra**, P; **R.B. Rosen**, Zeavision (F), Genentech (F), Opko-OTI (C), Optos (C), Clarity (C), OD-OS (C), Optovue (C), Topcon (R)

References

1. Ashton N. Retinal micro-aneurysms in the non-diabetic subject. *Br J Ophthalmol*. 1951;35:189–212.
2. Ashton N. Studies of the retinal capillaries in relation to diabetic and other retinopathies. *Br J Ophthalmol*. 1963;47:521–538.
3. Factor SM, Okun EM, Minase T. Capillary microaneurysms in the human diabetic heart. *N Engl J Med*. 1980;302:384–388.
4. Russell RW. How does blood-pressure cause stroke? *Lancet*. 1975;2:1283–1285.
5. Bloodworth JM Jr. A re-evaluation of diabetic glomerulosclerosis 50 years after the discovery of insulin. *Hum Pathol*. 1978;9:439–453.
6. Wong TY, Klein R, Sharrett AR, et al. Retinal microvascular abnormalities and cognitive impairment in middle-aged persons: the Atherosclerosis Risk in Communities Study. *Stroke*. 2002;33:1487–1492.
7. Wong TY, McIntosh R. Hypertensive retinopathy signs as risk indicators of cardiovascular morbidity and mortality. *Br Med Bull*. 2005;73-74:57–70.
8. Cooper LS, Wong TY, Klein R, et al. Retinal microvascular abnormalities and MRI-defined subclinical cerebral infarction: the Atherosclerosis Risk in Communities Study. *Stroke*. 2006;37:82–86.
9. Baker ML, Hand PJ, Wang JJ, Wong TY. Retinal signs and stroke: revisiting the link between the eye and brain. *Stroke*. 2008;39:1371–1379.
10. Wong TY, Klein R, Sharrett AR, et al. Cerebral white matter lesions, retinopathy, and incident clinical stroke. *JAMA*. 2002;288:67–74.
11. Yu T, Mitchell P, Berry G, Li W, Wang JJ. Retinopathy in older persons without diabetes and its relationship to hypertension. *Arch Ophthalmol*. 1998;116:83–89.
12. Ishikawa K, Uyama M, Asayama K. Occlusive thromboaortopathy (Takayasu's disease): cervical arterial stenoses, retinal arterial pressure, retinal microaneurysms and prognosis. *Stroke*. 1983;14:730–735.

13. Wilkinson CP, Ferris FL III, Klein RE, et al. Proposed international clinical diabetic retinopathy and diabetic macular edema disease severity scales. *Ophthalmology*. 2003;110:1677–1682.
14. Hirai FE, Moss SE, Knudtson MD, Klein BE, Klein R. Retinopathy and survival in a population without diabetes: the Beaver Dam Eye Study. *Am J Epidemiol*. 2007;166:724–730.
15. Grading diabetic retinopathy from stereoscopic color fundus photographs—an extension of the modified Airlie House classification. ETDRS report number 10. Early Treatment Diabetic Retinopathy Study Research Group. *Ophthalmology*. 1991;98:786–806.
16. Fundus photographic risk factors for progression of diabetic retinopathy. ETDRS report number 12. Early Treatment Diabetic Retinopathy Study Research Group. *Ophthalmology*. 1991;98:823–833.
17. Klein R, Meuer SM, Moss SE, Klein BE. Retinal microaneurysm counts and 10-year progression of diabetic retinopathy. *Arch Ophthalmol*. 1995;113:1386–1391.
18. Sjolie AK, Klein R, Porta M, et al. Retinal microaneurysm count predicts progression and regression of diabetic retinopathy. Post-hoc results from the DIRECT Programme. *Diabet Med*. 2011;28:345–351.
19. Csaky KG, Richman EA, Ferris FL III. Report from the NEI/FDA Ophthalmic Clinical Trial Design and Endpoints Symposium. *Invest Ophthalmol Vis Sci*. 2008;49:479–489.
20. Klein R, Meuer SM, Moss SE, Klein BE. The relationship of retinal microaneurysm counts to the 4-year progression of diabetic retinopathy. *Arch Ophthalmol*. 1989;107:1780–1785.
21. Kohner EM, Sleightholm M. Does microaneurysm count reflect severity of early diabetic retinopathy? *Ophthalmology*. 1986;93:586–589.
22. Ribeiro ML, Nunes SG, Cunha-Vaz JG. Microaneurysm turnover at the macula predicts risk of development of clinically significant macular edema in persons with mild nonproliferative diabetic retinopathy. *Diabetes Care*. 2013;36:1254–1259.
23. Nunes S, Pires I, Rosa A, Duarte L, Bernardes R, Cunha-Vaz J. Microaneurysm turnover is a biomarker for diabetic retinopathy progression to clinically significant macular edema: findings for type 2 diabetics with nonproliferative retinopathy. *Int J Ophthalmol*. 2009;223:292–297.
24. Bernardes R, Nunes S, Pereira I, et al. Computer-assisted microaneurysm turnover in the early stages of diabetic retinopathy. *Int J Ophthalmol*. 2009;223:284–291.
25. Goatman KA, Cree MJ, Olson JA, Forrester JV, Sharp PF. Automated measurement of microaneurysm turnover. *Invest Ophthalmol Vis Sci*. 2003;44:5335–5341.
26. Kohner EM, Stratton IM, Aldington SJ, Turner RC, Matthews DR. Microaneurysms in the development of diabetic retinopathy (UKPDS 42). UK Prospective Diabetes Study Group. *Diabetologia*. 1999;42:1107–1112.
27. Murakami T, Nishijima K, Sakamoto A, Ota M, Horii T, Yoshimura N. Foveal cystoid spaces are associated with enlarged foveal avascular zone and microaneurysms in diabetic macular edema. *Ophthalmology*. 2011;118:359–367.
28. Cogan DG, Toussaint D, Kuwabara T. Retinal vascular patterns. IV. Diabetic retinopathy. *Arch Ophthalmol*. 1961;66:366–378.
29. de Oliveira F. Pericytes in diabetic retinopathy. *Br J Ophthalmol*. 1966;50:134–143.
30. Ashton N. Vascular basement membrane changes in diabetic retinopathy. Montgomery lecture, 1973. *Br J Ophthalmol*. 1974;58:344–366.
31. Wise G. Retinal microaneurysms. *Arch Ophthalmol*. 1957;151–156.
32. Yanoff M, Fine BS. *Ocular Pathology: A Text and Atlas*. Hagerstown: Harper & Row; 1975.
33. Bresnick GH, Davis MD, Myers FL, de Venecia G. Clinicopathologic correlations in diabetic retinopathy. II. Clinical and histologic appearances of retinal capillary microaneurysms. *Arch Ophthalmol*. 1977;95:1215–1220.
34. Stitt AW, Gardiner TA, Archer DB. Histological and ultrastructural investigation of retinal microaneurysm development in diabetic patients. *Br J Ophthalmol*. 1995;79:362–367.
35. Moore J, Bagley S, Ireland G, McLeod D, Boulton ME. Three dimensional analysis of microaneurysms in the human diabetic retina. *J Anat*. 1999;194(pt 1):89–100.
36. Ezra E, Keinan E, Mandel Y, Boulton ME, Nahmias Y. Non-dimensional analysis of retinal microaneurysms: critical threshold for treatment. *Integr Biol*. 2013;5:474–480.
37. Kozak I, Oster SF, Cortes MA, et al. Clinical evaluation and treatment accuracy in diabetic macular edema using navigated laser photocoagulator NAVILAS. *Ophthalmology*. 2011;118:1119–1124.
38. Burgansky-Eliash Z, Barak A, Barash H, et al. Increased retinal blood flow velocity in patients with early diabetes mellitus. *Retina*. 2012;32:112–119.
39. Burgansky-Eliash Z, Nelson DA, Bar-Tal OP, Lowenstein A, Grinvald A, Barak A. Reduced retinal blood flow velocity in diabetic retinopathy. *Retina*. 2010;30:765–773.
40. Nelson DA, Burgansky-Eliash Z, Barash H, et al. High-resolution wide-field imaging of perfused capillaries without the use of contrast agent. *Clin Ophthalmol*. 2011;5:1095–1106.
41. Srinivasan VJ, Adler DC, Chen Y, et al. Ultrahigh-speed optical coherence tomography for three-dimensional and en face imaging of the retina and optic nerve head. *Invest Ophthalmol Vis Sci*. 2008;49:5103–5110.
42. Schmoll T, Singh ASG, Blatter C, et al. Imaging of the parafoveal capillary network and its integrity analysis using fractal dimension. *Biomed Opt Express*. 2011;2:1159–1168.
43. Zhi Z, Yin X, Dziennis S, et al. Optical microangiography of retina and choroid and measurement of total retinal blood flow in mice. *Biomed Opt Express*. 2012;3:2976–2986.
44. Kim DY, Fingler J, Werner JS, Schwartz DM, Fraser SE, Zawadzki RJ. In vivo volumetric imaging of human retinal circulation with phase-variance optical coherence tomography. *Biomed Opt Express*. 2011;2:1504–1513.
45. Kim DY, Fingler J, Zawadzki RJ, et al. Noninvasive imaging of the foveal avascular zone with high-speed, phase-variance optical coherence tomography. *Invest Ophthalmol Vis Sci*. 2012;53:85–92.
46. Zotter S, Pircher M, Torzicky T, et al. Visualization of microvasculature by dual-beam phase-resolved Doppler optical coherence tomography. *Opt Express*. 2011;19:1217–1227.
47. Bradley A, Zhang H, Applegate RA, Thibos LN, Elsner AE. Entoptic image quality of the retinal vasculature. *Vision Res*. 1998;38:2685–2696.
48. Yap M, Gilchrist J, Weatherill J. Psychophysical measurement of the foveal avascular zone. *Ophthalmic Physiol Opt*. 1987;7:405–410.
49. Bird AC, Weale RA. On the retinal vasculature of the human fovea. *Exp Eye Res*. 1974;19:409–417.
50. Wang H, Chhablani J, Freeman WR, et al. Characterization of diabetic microaneurysms by simultaneous fluorescein angiography and spectral-domain optical coherence tomography. *Am J Ophthalmol*. 2012;153:861–867.
51. Rha J, Jonnal RS, Thorn KE, Qu J, Zhang Y, Miller DT. Adaptive optics flood-illumination camera for high speed retinal imaging. *Opt Express*. 2006;14:4552–4569.
52. Lombardo M, Parravano M, Serrao S, Ducoli P, Stirpe M, Lombardo G. Analysis of retinal capillaries in patients with

Investigative Ophthalmology & Visual Science

type 1 diabetes and nonproliferative diabetic retinopathy using adaptive optics imaging. *Retina*. 2013;33:1630–1639.

53. Chui TY, Vannasdale DA, Burns SA. The use of forward scatter to improve retinal vascular imaging with an adaptive optics scanning laser ophthalmoscope. *Biomed Opt Express*. 2012;3: 2537–2549.
54. Chui TY, Zhong Z, Song H, Burns SA. Foveal avascular zone and its relationship to foveal pit shape. *Optom Vis Sci*. 2012; 89:602–610.
55. Tam J, Martin JA, Roorda A. Noninvasive visualization and analysis of parafoveal capillaries in humans. *Invest Ophthalmol Vis Sci*. 2010;51:1691–1698.
56. Tam J, Dhamdhere KP, Tiruveedhula P, et al. Disruption of the retinal parafoveal capillary network in type 2 diabetes before the onset of diabetic retinopathy. *Invest Ophthalmol Vis Sci*. 2011;52:9257–9266.
57. Chui TY, Gast TJ, Burns SA. Imaging of vascular wall fine structure in human retina using adaptive optics scanning laser ophthalmoscopy. *Invest Ophthalmol Vis Sci*. 2013;54:7115–7124.
58. Miller DT, Kocaoglu OP, Wang Q, Lee S. Adaptive optics and the eye (super resolution OCT). *Eye*. 2011;25:321–330.
59. Wang Q, Kocaoglu OP, Cense B, et al. Imaging retinal capillaries using ultrahigh-resolution optical coherence tomography and adaptive optics. *Invest Ophthalmol Vis Sci*. 2011;52:6292–6299.
60. Pinhas A, Dubow M, Shah N, et al. In vivo imaging of human retinal microvasculature using adaptive optics scanning light ophthalmoscope fluorescein angiography. *Biomed Opt Express*. 2013;4:1305–1317.
61. Smith G, Atchison DA. *The Eye and Visual Optical Instruments*. 1st ed. Cambridge: Cambridge University Press; 1997.
62. Dubra A, Sulai Y. Reflective afocal broadband adaptive optics scanning ophthalmoscope. *Biomed Opt Express*. 2011;2: 1757–1768.
63. Delori FC, Webb RH, Sliney DH. American National Standards I. Maximum permissible exposures for ocular safety (ANSI 2000), with emphasis on ophthalmic devices. *J Opt Soc Am A*. 2007;24:1250–1265.
64. Dubra A, Harvey Z. *Registration of 2D Images from Fast Scanning Ophthalmic Instruments The 4th International Workshop on Biomedical Image Registration*. Lübeck; Springer Berlin Heidelberg; 2010.
65. Fleiss JL, Levin B, Paik MC. *Statistical Methods for Rates and Proportions*. 3rd ed. New York: John Wiley & Sons; 2003.
66. Tam J, Dhamdhere KP, Tiruveedhula P, et al. Subclinical capillary changes in non-proliferative diabetic retinopathy. *Optom Vis Sci*. 2012;89:E692–E703.
67. Srinivasan VJ, Radhakrishnan H, Lo EH, et al. OCT methods for capillary velocimetry. *Biomed Opt Express*. 2012;3:612–629.
68. Braaf B, Vienola KV, Sheehy CK, et al. Real-time eye motion correction in phase-resolved OCT angiography with tracking SLO. *Biomed Opt Express*. 2013;4:51–65.
69. Jia Y, Morrison JC, Tokayer J, et al. Quantitative OCT angiography of optic nerve head blood flow. *Biomed Opt Express*. 2012;3:3127–3137.
70. Asari S, Ohmoto T. Natural history and risk factors of unruptured cerebral aneurysms. *Clin Neurol Neurosurg*. 1993;95:205–214.
71. Wiebers DO, Whisnant JP, O'Fallon WM. The natural history of unruptured intracranial aneurysms. *N Engl J Med*. 1981;304: 696–698.
72. Sampei T, Mizuno M, Nakajima S, et al. Clinical study of growing up aneurysms: report of 25 cases. *Neurol Med Chir*. 1991;19:825–830.
73. Hademenos GJ, Massoud TF, Turjman F, Sayre JW. Anatomical and morphological factors correlating with rupture of intracranial aneurysms in patients referred for endovascular treatment. *Neuroradiology*. 1998;40:755–760.

Investigative Ophthalmology & Visual Science